Delft University of Technology

A study on siting of emergency shelters for dam failure floods considering population distribution and weather effects

Jiao, Yutie; Li, Zongkun; Ge, Wei; Jing, Laihong; Wu, Meimei; Wang, Te; Sun, Heqiang; Wang, Jianyou; Zhang, Xiangyang; van Gelder, Pieter

Important note
To cite this publication, please use the final published version (if applicable).
Please check the document version above.

A study on siting of emergency shelters for dam failure floods considering population distribution and weather effects

Yutie Jiao [a,b], Zongkun Li [a,b], Wei Ge [a,b,c,*], Laihong Jing [c], Meimei Wu [d], Te Wang [a,b], Heqiang Sun [a,b], Jianyou Wang [a,b], Xiangyang Zhang [a,b], Pieter van Gelder [e]

[a] School of Water Conservancy and Transportation, Zhengzhou University, Zhengzhou 450001, PR China
[b] Yellow River Laboratory, Zhengzhou University, Zhengzhou 450001, PR China
[c] Yellow River Engineering Consulting Co., Ltd., Zhengzhou 450003, PR China
[d] College of Civil Engineering and Architecture, Henan University of Technology, Zhengzhou 450001, PR China
[e] Safety and Security Science Group (S3G), Faculty of Technology, Policy and Management, Delft University of Technology, Delft 2628 BX, the Netherlands

HIGHLIGHTS

- People distribution and weather have significant effects on shelter selection.
- The capacity and accessibility of shelters vary with the weather.
- Shelters have been allocated for populations with different evacuation methods.

GRAPHICAL ABSTRACT
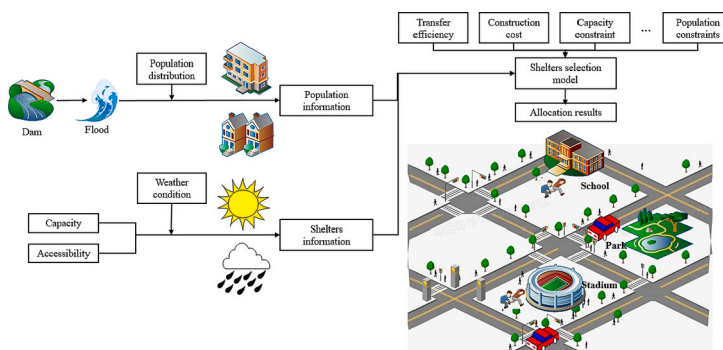
ARTICLE INFO

ABSTRACT

In recent years, dam failures have occurred frequently because of extreme weather, posing a significant threat to downstream residents. The establishment of emergency shelters is crucial for reducing casualties. The selection of suitable shelters depends on key information such as the number and distribution of affected people, and the effective capacity and accessibility of the shelters. However, previous studies on siting shelters did not fully consider population distribution differences at a finer scale. This limitation hinders the accuracy of estimating the number of affected people. In addition, most studies ignored the impact of extreme rainfall on the effective capacity and accessibility of shelters, leading to a low applicability of the shelter selection results. Therefore, in this study, land-use and land-cover change (LUCC) and nighttime lighting data were used to simulate population distribution and determine the number and distribution of affected people. Qualified candidate shelters were obtained based on screening criteria, and their effective capacity and accessibility information under different weather conditions were quantified. Considering factors such as population transfer efficiency, construction cost and shelter capacity constraints, a multi-objective siting model was established and solved using the non-dominated sorting genetic algorithm II (NSGA- II) to obtain the final siting scheme. The method was applied

* Corresponding author at: School of Water Conservancy and Transportation, Zhengzhou University, Zhengzhou 450001, PR China.
  E-mail address: gewei@zzu.edu.cn (W. Ge).

to the Dafangying Reservoir, and the results showed the following: (1) The overall mean relative error (MRE) of the population in the 35 downstream streets was 11.16 %, with good fitting accuracy. The simulation results truly reflect the population distribution. (2) Normal weather screening generated 352 qualified candidate shelters, whereas extreme rainfall weather screening generated 266 candidate shelters. (3) Based on the population distribution and weather factors, four scenarios were set up, with 63, 106, 73, and 131 shelters selected. These two factors have a significant impact on the selection of shelters and the allocation of evacuees, and should be considered in the event of a dam-failure floods.

1. Introduction

Increasing global temperatures have contributed to a higher frequency of extreme rainfall events (Wu et al., 2021; Kreibich et al., 2022; Kotz et al., 2022); combined with many reservoir dams that have been built for a long time and have poor operational management, this leads to dam breaches occurring worldwide (Ge et al., 2021, 2022; Zhu and Tang, 2023), posing significant threats to the safety of downstream residents (Zhang et al., 2023a, 2023b; Lv et al., 2022; Ge et al., 2020a, 2020b). In May 2020, the Edenville and Sanford dams in the United States collapsed successively, resulting in the emergency evacuation of over 10,000 residents (Wang et al., 2022a, 2022b; Wang et al., 2023a, 2023b). In the same month, the Sardoba Reservoir in Uzbekistan failed, causing 5 deaths, over 50 injuries, and the evacuation of >70,000 people (Li et al., 2021a, 2021b). In July 2021, the Yong'an and Xinfa reservoirs in Inner Mongolia, China, were breached, leading to the emergency evacuation of over 1400 people (Wang et al., 2023a, 2023b). Additionally, the "7–20" heavy rainfall in Zhengzhou endangered the Guojiazui Reservoir, Changzhuang Reservoir, and downstream embankments of the Jialu River, resulting in the emergency evacuation of hundreds of thousands of people (Zhang et al., 2023a, 2023b). With social and economic development, the population protected by dams has increased, rendering the consequences of dam failures increasingly unacceptable (Li et al., 2018; Ge et al., 2017, 2022). As a preparatory measure for disaster prevention and mitigation, urban emergency shelters play a crucial role in reducing casualties (Baharmand et al., 2019). Therefore, the scientific siting of emergency shelters to efficiently satisfy the evacuation requirements of residents and management requirements of the government is an inevitable choice to enhance the ability of cities to respond to sudden disasters and accidents. It is also an important part of the construction and improvement of the city's public safety and emergency management system (Felice et al., 2021; Ottavia et al., 2021).

Modern site selection research originated in 1909, Weber (1929) was the first to propose the problem of minimizing the total distance from a single warehouse site to multiple customers, which initiated a theoretical study of the site selection problem. Later, the introduction of the p-median (Hakimi, 1964), p-center (Hakimi, 1965), set covering (Toregas et al., 1971), and maximum covering models (Church and Revelle, 1974), marked the beginning of the shift towards a systematic approach in siting studies. Over the years, researchers have extensively applied and improved these four models by incorporating various considerations and refining the application scenarios. For instance, Wood and Schmidtlein. (2013) analyzed the evacuation potential of populations under tsunami threats and proposed the creation of vertical shelters in areas with difficult evacuation. Kilci et al. (2015) determined the weight of each shelter by considering factors such as transportation status, evacuation distance and minimum utilization rate of the site, and then constructed a site selection model for earthquake. Esmaelian et al. (2015) used geographic information system (GIS) and multi-criteria decision-making methods to develop a shelter selection model that considered seismic grade, building age, and population density; they was applied to the Tehran region. Zhao et al. (2017) studied the relationship between evacuation time and total shelter area under different population sizes and used an improved particle swarm algorithm to solve the seismic shelter siting problem. Yao et al. (2017) proposed a

dual objective model for optimizing the siting of urban fire stations, considering service coverage, accessibility, and the impact of existing fire stations. Qin et al. (2020) considered the variation of typhoon paths and developed an emergency evacuation model by using an improved particle swarm algorithm. Rahman et al. (2020) developed a model for optimizing the spatial distribution of emergency evacuation centers by analyzing the sensitivity of flooding in the Sylhet area of Bangladesh to help reduce casualties, and property damage, and improve emergency operations. Baharmand et al. (2020) considered factors such as coverage range, logistics costs, and response time to establish a model for the site selection of temporary relief distribution centers; they validated the method with the example of the 2015 Nepal earthquake. Geng et al. (2021) developed a dual-objective hierarchical model consisting of two stages, namely the temporary shelter and the short-term shelter stages, offering dependable solutions for shelter site selection and material distribution in Chengdu, China. Zhong et al. (2022) combined static network analysis with dynamic evacuation simulation and used genetic algorithms to plan shelters in the central urban area of Xinyi City, China.

Population distribution is a crucial factor in assessing the number of affected people. However, most studies on site selection are based solely on official statistics to determine the number of people affected by a disaster without sufficiently considering the differences in population distribution at a finer scale. This limitation is particularly pronounced in China where publicly available census data are generally based on districts and counties with large spatial scales. Because the inundation area of a dam-failure floods does not align with administrative boundaries, if differences in population distribution are not considered, a significant discrepancy would occur between the estimated and actual number of affected people. In addition, the shelter requirements of the affected populations vary depending on the type of disaster. For example, for earthquakes, shelters should be set up in parks, squares, and other open spaces outside collapsed buildings. For dam failure floods, because extreme rainfall is one of the main causes of dam failure (Alessia et al., 2023), shelters should be well protected against rainfall and flooding when a dam fails under extreme rainfall weather. However, current siting studies have paid insufficient attention to dam-failure floods (Ozbay et al., 2019) and weather impacts, resulting in some planned shelters being limited by their elevation or spatial morphology. This makes it difficult to satisfy the sheltering requirements of populations under extreme rainfall weather conditions. To address these challenges, this study aimed to compare and analyze the effects of population distribution and weather condition on shelters selection. The findings of this study can provide valuable insights for emergency managers and a reference for selecting suitable shelters.

Additionally, we emphasize that, as a social public facility, the investment, construction, and planning of shelters are primarily determined by the government. Therefore, site selection should be approached not only from a mathematical perspective by adding constraints or optimizing objectives but also from a policy and strategic perspective (Trivedi, 2018). For instance, with the intensification of global climate change and increasing environmental concerns, many countries have joined low-carbon development teams to address global environmental crises in, which sustainable development plays an increasingly crucial role in government decision-making (Sun et al., 2022). However, owing to the different carbon emission patterns and levels among countries, their corresponding sustainable development

policies and progress also differ (Jakovljevic et al., 2020), thus requiring different focus areas in shelter selection for different countries. Most economically developed countries in the Organization for Economic Co-operation and Development (OECD) have established good examples of low-carbon development (Jeong et al., 2021). Many BRICS countries actively promote low-carbon development through policy support, technological innovation, and structural energy adjustments (Jakovljevic et al., 2022, 2023). Therefore, integrating low-carbon considerations will become a popular topic in siting research in these countries (Maryam et al., 2023), and will facilitate the implementation of siting schemes. However, some low-income and middle-income countries influenced by limited national economic and social capital may prioritize economic growth at the expense of resources and the environment (Allahham et al., 2022). Currently, a low-carbon prioritization strategy may lead to inappropriate prioritization settings and strategic plans (Ranabhat et al., 2020). Thus, minimizing investment costs while satisfying population requirements is crucial for implementing siting schemes in these countries. While policy considerations are not the primary focus of this paper, we call upon researchers to give it due attention to promote the implementation of siting scheme.

2. Materials and methods

2.1. Study areas

The Dafang Ying Reservoir (31.93 N, 117.24 E) is located in Hefei City, Anhui Province, China, along the Sili River, a tributary of the Nanfei River. It serves as a large (II) type reservoir primarily for floods control and urban water supply. The reservoir consists of a main dam, sub-dam, spillway and discharge culvert. The main dam spans 2135 m, and the sub-dam spans 1703 m, all of which are roller-compacted homogeneous earth dams. The reservoir basin has an area of 184 km², total capacity of 184 million m³, 500-year floods design, design water level of 30.74 m, probable maximum floods (PMF) standard check, and check water level of 33.64 m. Notably, the main dam is only 5 km from the city center and is the closest large reservoir in China to its capital city (Hefei), supporting the city along with the Dongpu Reservoir. Hefei City falls within a humid monsoon climate zone and experiences significant spatial and temporal variations in rainfall. Influenced by cold fronts, low

vortices, typhoons, and other factors, the region experiences concentrated rainfall in summer, frequent rainstorms, and floods. Therefore, Hefei has been listed as one of the 31 key floods control cities in China. Downstream of the reservoir are the districts of Luyang, Shushan, Yaohai, and Baohe in Hefei City, and the population is concentrated in the middle-terrain and low-terrain areas with convenient transportation and a developed economy, whereas the population distribution in the high-terrain areas is lower, and the spatial distribution of the population is considerably different. An overview of the study area is shown in Fig. 1.

2.2. Site selection process

Site selection is a complex process that involves considering various factors and adapting them to local scenarios. Regardless of specific circumstances, accurate information on the number of people affected by disasters and the capacity and accessibility of shelters should be obtained, as these data form the basis for shelter selection. During a dam-failure floods event, the first step in the shelter selection process is to determine the number and distribution of the affected population. As the population is not uniformly distributed geospatially, its precise number and distribution should be determined in combination with population distribution simulations. When the affected populations have been identified, the next step is to screen candidate shelters that satisfy specific basic criteria, such as safety and efficacy, and collect information on the geographic location, effective capacity, and accessibility of these shelters (that some information may change owing to weather conditions) to support the subsequent determination of the final shelters. Finally, a mathematical model for shelter selection should be established based on certain objectives and constraints, taking the above information on the affected population and candidate shelters as inputs to the model and using an algorithm to solve the model to realize shelter selection and the population allocation. The shelters selection process for the dam-failure floods is shown in Fig. 2.

2.3. Numerical simulation of dam failure floods

Dam failure floods simulations can be used to determine potential inundation areas downstream of a dam. In this study, the HEC-RAS hydrodynamic model was used to simulate dam failure flooding (US
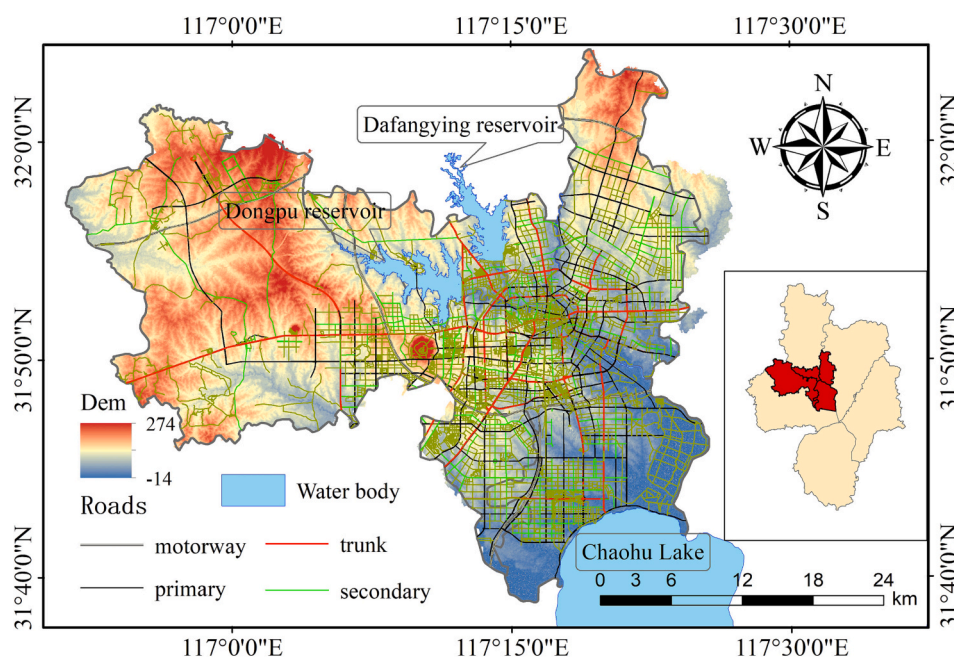

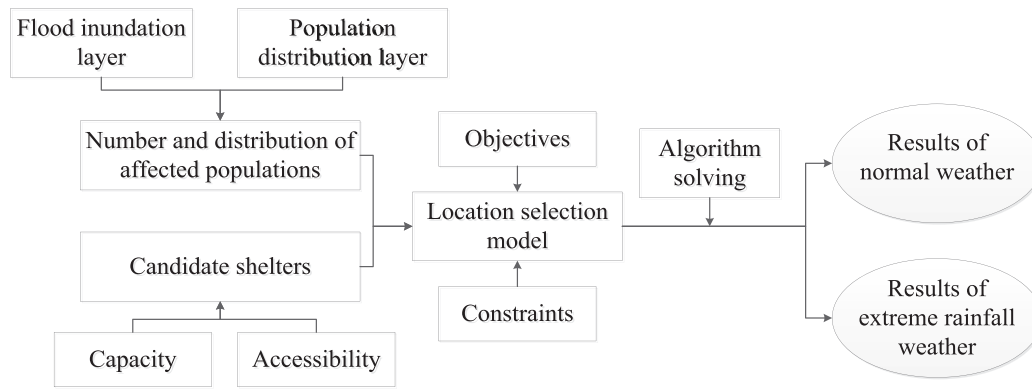**Fig. 1.** Overview of the study area.

Fig. 2. The process of selecting dam failure floods shelters.

Army Corps of Engineers, Hydrologic Engineering Center, 2016). Assuming that the dam breaches through overtopping, according to Xu and Zhang (2009), we set the top width, bottom width, height and breach time of the breach to 123 m, 90 m, 16.1 m and 6.9 h, respectively. The duration of the simulation was set to 24 h. The data used in the simulation process included a 30 m resolution digital elevation model (DEM) (used to reflect the topographic and geomorphological changes in the downstream area) and 30 m resolution land-use and land-cover change (LUCC) data (used to set the corresponding roughness).

2.4. Simulation of population distribution

Population distribution modeling can be used to determine the number and distribution of a population downstream of a reservoir. Traditionally, demographic data have been the primary method of obtaining population numbers. However, this method has the following problems in practical applications (Wang et al., 2018; Bao et al., 2023): (1) Population statistics are often based on administrative divisions, with a large spatial scale, and the population distribution within administrative units cannot be reflected. (2) The boundaries of administrative areas do not align with floods inundation boundaries, making it difficult to accurately estimate the affected population. Population distribution simulation at the grid scale provides an effective solution to address these problems. Advancements in remote-sensing technology have facilitated the use of remote sensing images in population spatial distribution studies, offering benefits such as easy accessibility, high accuracy, and wide coverage (Weber et al., 2018; Chen et al., 2023). A significant correlation between nighttime lighting and LUCC data in remote-sensing images and population distribution has been confirmed, which has significant potential for characterizing population spatial distribution (Li et al., 2018; Fang et al., 2022). Nighttime light data from sources such as DMSP/OLS, NPP/VIIRS, and Luojia-1, as well as LUCC data such as Globeland30 and WorldCover, have achieved global coverage and can be utilized in any city or country. This study used the 30 m resolution LUCC data from Hefei City in 2020 (Center for Resource and Environmental Science and Data, 2020) and the 130 m resolution nighttime light data provided by the Luo Jia 1 satellite (State Key Laboratory of Surveying and Mapping and Remote Sensing, Wuhan University, n.d.) simulate the population distribution.

The unified coordinate system was WGS 1984 UTM Zone 50 N, and the grid size was set to 130 m, which is consistent with the accuracy of the nighttime lighting data. Due to the LUCC are discrete geographic data with intermittent distribution characteristics, they were resampled to 130 m using the nearest-neighbor method (Bahareh et al., 2020; Lv et al., 2021). The first level classification of LUCC data was used as a modeling factor, excluding watersheds and unused land, which have low relevance to population activities. Cropland, forest land, grassland, and urban and construction land were selected as population modeling factors.

2.4.1. Progressive regression fitting

Land is a carrier of the population, and LUCC data can indicate the population distribution of different land types. However, it fails to capture variations in population distribution within the same type of land. This limitation can be addressed by using nighttime lighting data to depict the internal variability (Wu et al., 2023). Therefore, with the above four land types, the area of lights on the land, and the intensity of the lights as independent variables, and the demographics as dependent variables, according to the principle that if there is no land, then there is no population, the constant term of the regression equation was set to 0, and the equation was established as shown in Eq. (1).

$$POP_i = \sum_{j=1}^{n}(a \cdot AL_{ij} + b \cdot IL_{ij}) \tag{1}$$

where: POP_i is the number of resident population in the ith township from the demographic data; j is the number of land use types; AL_{ij} and IL_{ij} are the area of lighted areas and the total intensity of light on the jth land type in the ith township, respectively; a, b are the regression coefficients.

Stepwise regression was employed to fit the data, and independent variables were retained if their coefficients were significant at a confidence level of 0.05. Furthermore, to ensure that the population on each grid was positive and to avoid inconsistencies with reality, independent variables with negative coefficients were removed each time the regression equation was created.

2.4.2. Zoning based on population agglomeration degree

The modeling concept of the above progressive regression fit is the assumption that the same type of land is equally attractive to the population. Differences in the attractiveness of the same type of land to the population were observed (Zhao et al., 2020). To enhance simulation accuracy, this study subdivided the study area using population agglomeration, which aided in capturing the variations in the attractiveness of the same land type in different regions (Tan et al., 2018). The calculation formula of the population agglomeration degree (Agg) is given by Eq. (2).

$$Agg_i = \frac{(P_i/P_n) \times 100\%}{(A_i/A_n) \times 100\%} = \frac{P_i/A_i}{P_n/A_n} \tag{2}$$

where: Agg_i is the agglomeration of street i; P_i is the population of street i; A_i is the area of street i; P_n is the total population of the study area; and A_n is the total area of the study area.

2.4.3. Evaluation of the fitting error

To evaluate the accuracy of the simulation results, R_2, relative error (RE) and mean relative error (MRE) were used to evaluate the fitting effect, and the calculation formulas are shown in Eqs. (3) to (5).

$$R^2 = \left(\frac{\sum_{i=1}^{n}(POP_i' - \overline{POP'})(POP_i - \overline{POP})}{\sqrt{\sum_{i=1}^{n}(POP_i' - \overline{POP'})^2}\sqrt{\sum_{i=1}^{n}(POP_i - \overline{POP})^2}} \right)^2 \tag{3}$$

$$RE = \frac{|POP_i - POP_i'|}{POP_i} \tag{4}$$

$$MRE = \frac{1}{n}\sum_{i=1}^{n}\frac{|POP_i - POP_i'|}{POP_i} \tag{5}$$

where: POP_i and POP_i' are the statistical and estimated population of street i, respectively; $\overline{POP}$ and $\overline{POP'}$ are the average of the statistical and estimated population of all streets in the region, respectively; and n is the number of streets in the region.

2.5. Screening and information quantification of candidate shelters

2.5.1. Selection criteria for candidate shelters

The final site selection results were generated from the qualified candidate shelters. Eligible sites from parks, plazas, green spaces, and schools in the study area were selected as candidate shelters using screening criteria based on safety, effectiveness, and connectivity requirements (Amini et al., 2022). Safety means that the shelters should be outside the potential inundation range of the dam-failure floods, and far from areas prone to geological hazards such as landslides, mudslides, seismic fault zones and storages of flammable and explosive explosives and poisonous gases to avoid the occurrence of secondary disasters. Effectiveness means that the capacity of the shelter should not be too small to avoid overcrowding, which could lead to stampedes, and difficulty for the government to unify the rescue and management of the population. Connectivity means that shelters should be set up in a place with flat terrain and a suitable slope to avoid restrictions on population transfer and medical assistance measures owing to the steepness of the terrain.

2.5.2. Quantification of effective capacity for shelters under different weather conditions

Extreme rainfall is one of the main causes of dam failure, and when a dam failures during extreme rainfall weather, the outdoor areas lack the necessary sheltering capabilities to effectively accommodate the affected population. Under normal weather conditions, both outdoor and indoor shelter areas are available to the affected population. Therefore, the capacity of each candidate shelter was subdivided into outdoor capacity C_o and indoor capacity C_i. C_o was based on the information provided by the Hefei Emergency Management Bureau and requirements of the GB51143–2015 (Code for Design of Disasters Mitigation Emergency Congregate Shelter), and a per capita effective area of 2 m^2/person was used to convert the measured outdoor area (measured from high-definition satellite maps and deleting fractional sites with insufficient plot widths) into capacity (it should be the normative requirement of each country). The indoor capacity C_i was converted based on the floorage, considering that the walls, tables and chairs in the building also take up a certain amount of area; the capacity was converted to 3 m^2/person (it should be valued according to each country). Under normal weather conditions, the effective capacity of the candidate sites is $C_{j1} = C_o + C_i$. However, during extreme rainfall, the effective capacity of the candidate site is $C_{j2} = C_i$.

2.5.3. Quantification of accessibility for shelters under different weather conditions

Accessibility is a core concern in shelter selection studies. Accessibility can be interpreted as the shortest time required for affected populations to reach a designated shelter. The longer the time, the worse the accessibility. The path that takes the shortest time to evacuate a settlement to a shelter is considered optimal. However, under different weather conditions, the optimal path is not necessarily the same. Even if the optimal path is the same, the time spent evacuating is not necessarily the same. This is because under extreme rainfall weather, roads leading to some lower-lying shelters may be flooded, rendering the original optimal path unavailable and requiring the affected people to take a longer time to reach the shelters by detouring or even losing accessibility to the shelters due to the total flooding of the surrounding roads. Rainfall also reduces driver's ability to perceive the surrounding environment, and forming a film of water between the road surface and the tires, reducing friction, which can cause changes in a vehicle's travel speed and increase evacuation time.

This study used an origin-destination (OD) matrix to quantify accessibility. In the OD matrix, the starting points are the settlements and the end points are the candidate shelters, which are connected through the actual road network. After a time attribute is assigned to each road (the time required for the affected population to pass through the road), the OD matrix can be solved using time as an impedance to obtain the shortest time required to evacuate from each residential area to each shelter. Therefore, the key is to assign time attributes to each road. As the evacuation method has a significant impact on the evacuation time, the two most common evacuation methods driving a car and walking were considered.

(1) Evacuation by cars

When driving a car to evacuate in normal weather, a road resistance function is introduced to quantify the relationship between the road travel time and road traffic load (Li et al., 2021a, 2021b). Commonly used road impedance functions include the Bureau of Public Road's (BPR) function, the Conical function from the University of Montreal in Canada, the Logit function from the Ministry of Transportation and Road Safety in Israel, and the Indian Highway Capacity Manual Model (IDCM) in India. According to different national conditions, suitable road-resistance functions should be selected or established, and in this study, the Conical function was selected. The Conical function is an improved version of the BPR function (fitted from a large amount of reliable data), that solves the problem caused by large β values in the BPR function. Owing to its strong applicability and simplicity, it is adopted by the well-known planning software EMME2. The Conical function is expressed in Eq. (6).

$$t_{a1} = \frac{L_a}{V_0}\left(2 + \sqrt{\beta^2(1 - x_a/C_a) + \alpha^2} - \beta(1 - x_a/C_a) - \alpha\right) \tag{6}$$

where: t_{a1} is the traveling time on road a in normal weather; L_a is the length of road a; V_0 is the design speed of road a; x_a is the traffic flow on road a; C_a is the actual capacity of road a; α and β are constants, they should be valued according to national conditions, taking $\alpha = 1.4$, $\beta = 1.8$ in China.

The value range of V_0 (which should be adjusted for different country scenarios) was based on the China JTG B01–2014 (Technical Standard of Highway Engineering) in Table 1. However, during an actual disaster evacuation, traveling speed may be influenced by factors such as pedestrian interference and road width. To account for these factors, we applied the coefficients of pedestrian interference (y_1) and road width (y_2) to adjust V_0, as expressed in Eq. (7). The value criteria for

Table 1
Design speeds corresponding to different types of roads.

Road type	Motorway/trunk	Primary roads	Secondary roads	Tertiary roads
Design speeds (km/h)	60–80	40–60	20–40	20–30
Setting in manuscript	60	40	30	20

coefficients y_1 and y_2 are listed in Tables 2 and 3, respectively. The corrected traveling time on road a is given by in Eq. (8).

$$V_0^{'} = V_0 y_1 y_2 \tag{7}$$

$$t_{a1} = \frac{L_a}{V_0^{'}} \left(2 + \sqrt{\beta^2(1 - x_a/C_a) + \alpha^2} - \beta(1 - x_a/C_a) - \alpha \right) \tag{8}$$

where: $V_0^{'}$ is the corrected design speed on road a.

x_a/C_a is the actual load capacity of road a, which is reflected in the road service level. According to JTG B01–2014 (Technical Standard for Highway Engineering), road service is categorized into six levels based on the state of traffic flow. These levels describe the changing stages of traffic flow, from free, stable, saturated, and forced flow. In this study, the service level of each section of the road was set to the fifth level of service, that is $x_a/C_a \in (0.9, 1]$. At this point, each section of the road reaches the maximum capacity of the operating state, and any interference in the traffic flow may cause long queues.

When driving a car during rainy weather, if the water on the road surpasses the height of the exhaust pipe, the car may stall. In China, the exhaust port of an average car is typically positioned 20–30 cm above ground. Therefore, roads with water depths exceeding 20 cm should not be designated as evacuation routes. Moreover, even if the road does not have standing water, rainfall can impair driver perception and diminish friction by creating a water film between the ground and tires. This can result in changes in the vehicle speed. Zhang et al. (2017) examined the impact of varying congestion levels and road conditions on travel speeds at different precipitation intensities; the results are shown in Eq. (9) and Table 4. Vehicle travel in rainy weather is also affected by pedestrian interference and road width; therefore, vehicle speeds and travel times in rainy weather can be calculated based on normal weather, as shown in Eqs. (10) and (11):

$$\Delta V = a \ln(I) + b \tag{9}$$

$$V_r = \frac{L_a}{t_{a1}} - \Delta V \tag{10}$$

$$t_{a2} = \frac{L_a}{V_r} \tag{11}$$

where: ΔV is the value of speed loss; I is the intensity of precipitation (mm/15 min); a and b are coefficients to be determined; V_r is the traveling speed on road "a" under rainfall weather; t_{a2} is the traveling time on road "a" under rainfall weather.

(2) Evacuation on foot

When evacuating on foot, the walking speed of individuals under normal weather conditions is influenced by various factors, including age, sex, height, health status, and emotions. Environmental factors such as slope and temperature, also play a role. During rainy weather, the depth of water on roads and rainfall intensity further affect the walking speed. Because of the multitude of factors affecting walking speed, establishing a detailed distinction between different population groups becomes difficult. Typically, healthy adults maintain a speed of 4.5 to 6 km/h, where elderly individuals and children tend to exhibit slower speeds. However, during the actual evacuation process, vulnerable groups, such as the elderly and children, may receive assistance from family members or prioritize other evacuation methods. To simplify

Table 3
Criteria for the value of the coefficient of the road width y_2.

Road width(m)	y_2	Road width(m)	y_2
2.5	0.50	(4.0, 4.5]	1.20
(2.5, 3.0]	0.75	(4.5, 5.0]	1.26
(3.0, 3.5]	1.00	(5.0, 5.5]	1.29
(3.5, 4.0]	1.11	>5.5	1.30

Table 4
Criteria for the values of a and b in the coefficient y_1.

Time periods	Road type	a	b
Peak hours	Motorway/trunk	3.015	9.888
	Primary roads	0.395	3.518
	Secondary roads/tertiary roads	0.393	2.574
Non-peak hours	Motorway/trunk	2.122	6.864
	Primary roads	1.407	2.528
	Secondary roads/tertiary roads	0.929	1.897
Free flow	Motorway/trunk	2.291	4.519
	Primary roads	1.432	1.899
	Secondary roads/tertiary roads	1.638	2.206

Note: In this study, it is assumed that the state of the road during the actual disaster evacuation is similar to that during peak hours. Therefore, the values of a and b on each type of road correspond to the peak hours.

calculations, we used a uniform walking speed of 5 km/h for the entire study population.

2.6. Shelter selection modeling and solving

2.6.1. Shelter selection objectives and constraints

We established the following mathematical model for site selection that considers factors such as site selection cost, population distribution, weather conditions, shelter capacity, accessibility, and the principle of centralized resettlement.

(1) Transfer efficiency objective

Population transfer efficiency is a crucial objective of shelter selection studies (Ashlea et al., 2023). The less time required for transfer, the more efficient the transfer. To maximize the transfer efficiency of the affected population, we establish an objective function F_1 that aims to minimize the total transfer time for all populations, as shown in Eqs. (12)–(15).

$$F_1 = min \sum_{i=1}^{M} \sum_{j=1}^{N} \left(Y_{ijc} P_{ijc} t_{ijc} + Y_{ijw} P_{ijw} t_{ijw} \right) \tag{12}$$

$$t_{ijc} \in \left\{ t_{ijc1}, t_{ijc2} \right\} \tag{13}$$

$$t_{ijw} \in \left\{ t_{ijw1}, t_{ijw2} \right\} \tag{14}$$

$$Y_{ijc}, Y_{ijw} \in \{1, 0\} \tag{15}$$

where: M denotes the number of settlements; N denotes the number of candidate shelters; P_{ijc} and P_{ijw} are the number of people in settlement i transferred to shelter j by driving cars and walking, respectively; t_{ijc} is the time when the affected people in settlement i arrive at shelter j by driving, under normal weather take t_{ijc1}, under extreme rainfall take t_{ijc2}; t_{ijw} is the time when the affected people in settlement i arrive at shelter j

Table 2
Criteria for the value of the coefficient of the pedestrian interference y_1.

Interference degree	Extremely serious	Serious	Moderate	General	Slight	None
y_1	0.5	0.6	0.7	0.8	0.9	1.0
Setting in manuscript	/	/	Tertiary roads	Secondary roads	Primary roads	Motorway/trunk

by walking, under normal weather take t_{ijw1}, under extreme rainfall take t_{ijw2}; Y_{ijc} and Y_{ijw} are decision variables, when the population of settlement i transfers to shelter j by driving (walking), $Y_{ijc} = 1(Y_{ijw} = 1)$, otherwise $Y_{ijc} = 0(Y_{ijw} = 0)$。 .

(2) Construction cost objective

Shelters are social and public facilities that are primarily funded by government approval and appropriation. The cost plays a crucial role in determining the feasibility of constructing such facilities. Reducing the number of shelters to be built not only reduces construction costs, but also saves daily management and maintenance costs. It is important to minimize these costs while ensuring effective transfer efficiency (Jin et al., 2021). Consequently, the objective function F_2 is considered as the minimum total number of shelters to be constructed, as shown in Eqs. (16) and (17).

$$F_2 = min \sum_{j=1}^{N} Q_j Y_j \qquad (16)$$

$$Y_j \in \{1, 0\} \qquad (17)$$

where: Q_j is the priority parameter for shelter site j to be selected; Y_j is the decision variable, $Y_j = 1$ when shelter site j is selected and 0 otherwise.

(3) Population transfer constraints

To ensure that each resident could be assigned to a shelter and transferred to different shelters, we set the constraints shown in Eq. (18). Considering the principle of batch transfer for resettlement, the number of people to be transferred is set to 100 K (where K is a natural number) as shown in Eqs. (19) and (20). The number of people transferred to each settlement can be calculated using Eq. (21).

$$\sum_{j=1}^{N} (P_{ijc} + P_{ijw}) = P_i, \forall i \in M \qquad (18)$$

$$100K = q_{ijc} \le P_{ijc}, \forall i \in M, \forall j \in N \qquad (19)$$

$$100K = q_{ijw} \le P_{ijw}, \forall i \in M, \forall j \in N \qquad (20)$$

$$P_i = \sum_{x=1}^{m} POP_{grid_x} \qquad (21)$$

where: P_i denotes the number of people in settlement i; q_{ijc} and q_{ijw} are the number of people in settlement i transferred to shelter j by driving and walking, respectively; m denotes the number of people in settlement i with m flooded grids; POP_{grid_x} denotes the number of people corresponding to the xth grid that was flooded, which was determined based on the population distribution simulation results mentioned above.

(4) Shelter capacity constraints

The number of people accommodated in each shelter should not exceed its effective capacity. Thus, constraints are established as shown in Eq. (22). Based on the above analysis, the effective capacity of the shelter differs according to different weather conditions, as shown in Eq. (23).

$$\sum_{i=1}^{M} P_{ij} \le C_j, \forall j \in N \qquad (22)$$

$$C_j \in \{C_{j1}, C_{j2}\} \qquad (23)$$

where: C_j is the capacity of shelter j, which is divided into two conditions: the effective capacity under normal weather conditions, C_{j1}, and the effective capacity under extreme rainfall weather, C_{j2}.

2.6.2. NSGA-II (Non-dominated Sorting Genetic Algorithm II) solves

This model is a non-deterministic polynomial (NP) problem, which refers to a problem with non-deterministic polynomial complexity. Genetic algorithms are a type of search algorithms constructed by mathematical simulation based on Darwin's proposed laws of evolution (survival of the fittest genetic mechanism) in the biological world, and are very effective for solving the NP problem in this type of optimization combination (Kaseb and Rahbar, 2022; Seyed et al., 2023). This study used the NSGA-II to solving the problem, which has the following advantages over the traditional genetic algorithm: ① Fast non-dominated sorting reduces computational complexity. ② Its elite strategy better retains good individuals in the evolutionary process, and rapidly improves the population level by storing all individuals in the population hierarchically. ③ The introduction of the crowding degree and crowding distance comparison operator, instead of a fitness strategy that requires an artificially specified sharing radius, enhances species population diversity.

The NSGA-II process for retaining elite strategies is shown in Fig. 3, and the concepts of dominance level and crowding degree are schematically depicted in Fig. 4. To make this easier to understand, we explain it using a more generalized example. For instance, we aim to design a car shape that reduces air resistance (*f*1) while increasing the comfort of driving (*f*2). However, these two objectives are contradictory (reducing the air resistance will reduce the comfort of driving). To determine a solution that does well in both aspects, the NSGA-II achieves the followings:

(1) Initialization. Randomly generate a set of initial solutions of size X, also called parent population P_t. Each solution represents a combination of parameters for the car shape design, which are assumed to be controlled by three parameters: car length *l*, car width *w*, and car height *h*.

(2) Crossover and mutation. Use crossover and mutation operations to generate a new set of solutions, also called the offspring population Q_t, of the same size as the P_t. The crossover operation generates new offspring solutions by combining some parts of the two parent solutions; for example, a single-point crossover between parent solutions P_1 (l_1, w_1, h_1) and P_2 (l_2, w_2, h_2) occurs at the second parameter position, generating new offspring solutions Q_1 (l_1, w_2, h_2) and Q_2 (l_2, w_1, h_1). Mutation enables one or more genes to be randomly selected and changed. For example, the parent solution P_3 (l_3, w_3, h_3) has a mutation in the car length gene l_3, which increases in value by 2 cm, generating a new offspring solution Q_3 (2 cm + l_3, w_3, h_3).

(3) Non-dominated sorting. Combine P_t and Q_t to form a new population R_t of size 2 X, and perform fast non-dominated ordering of all solutions in R_t until all solutions are classified into the corresponding ranks (e.g., *L*1 and *L*2 in Fig. 4). For example, comparing the dominance relationship between R_1 (l_1, w_1, h_1) and R_2 (l_2, w_2, h_2) in R_t, if R_1 (l_1, w_1, h_1) better than R_2 (l_2, w_2, h_2) in both objectives (reducing air resistance, improving driving comfort), or when it is equal in one objective and better in another objective, it is denoted as R_1 (l_1, w_1, h_1) dominates R_2 (l_2, w_2, h_2).

(4) Calculate the crowding degree distance. The crowding degree distance represents the distribution density of a solution in the solution space, which is determined by measuring the distance between a solution and its neighboring solutions, as in Fig. 4 where the cuboid represents the crowding degree of solution i. The larger the crowding degree distance of a solution, the more distinctive it is, and we aim to maintain it to increase the diversity of the population and produce better offspring.
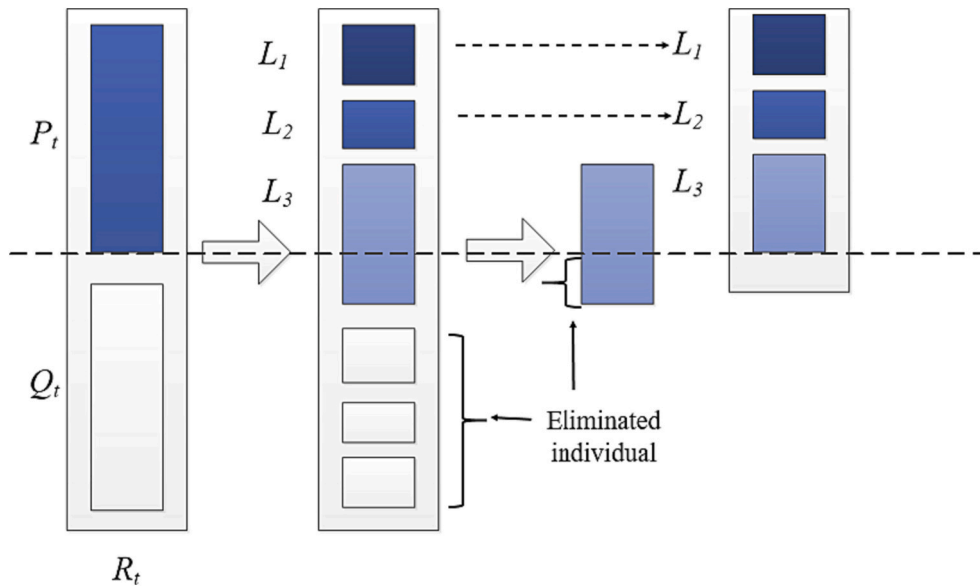
Fig. 3. Schematic diagram of the elite retention strategy of the NSGA-II algorithm.
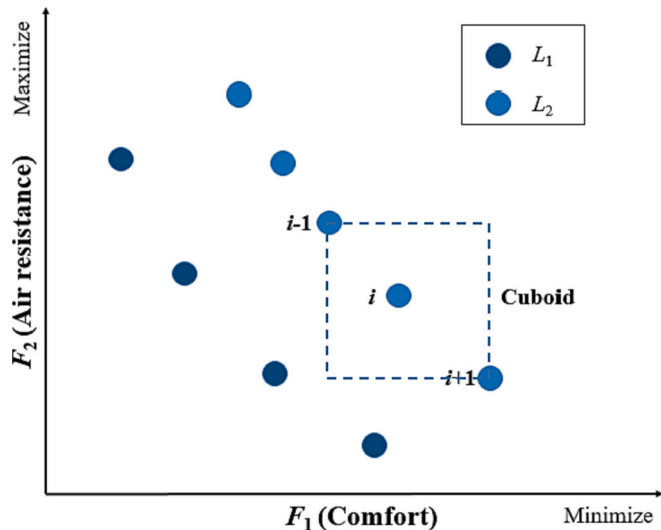

Fig. 4. Schematic diagram of the concepts of dominance level and crowding degree.

(5) Selection and filling. Individuals in the excellent dominance level ($L1$) are selected to be placed into the R_{t+1} generation first. When the number of individuals placed into a level (e.g., $L3$ in Fig. 3) exceeds the limit of X, individuals at that level with greater crowding (e.g., solution i in Fig. 4) are selected to be filled in until the population R_{t+1} size reaches X.

(6) Evolutionary iteration. Repeat steps (2) to (5); each generation of the population gradually evolves to produce a better solution set until the final result stabilizes and the program satisfies the termination condition.

3. Result

3.1. Results of simulation of dam failure floods and population distribution

According to the results of the dam-failure floods simulation, 26 streets (townships) in the study area were within the potential

inundation range of the dam failure-floods. To ensure that the samples were sufficient for modeling in each sub-district after partitioning, the number of streets was increased to 35, and the study area was divided into four sub-districts; A, B, C, and D. The streets they contains are A1 (Silihe Street), A2 (Xinghuacun Street), A3 (Hongguang Street), A4 (Wanghu Street), A5 (Feihe Town), A6 (Daxing Town), A7 (Luyang Economic and Technological Development Zone), A8 (Changqing Street), A9 (Luogang Street), A10 (Dayang Town), A11 (Jinggang Town), A12 (Qilitang Street), B1 (Jiashan Street), B2 (Sanxiaokou Street), B3 (Xiaoyaojin Street), B4 (Daoxiangcun Street), B5 (Chengdong Street), B6 (Sanli'an Street), B7 (Fangmiao Street), C1 (Tongling Street), C2 (Qilizhan Street), C3 (Changhuai Street), C4 (Hupo Street), C5 (Xiyuan Street), C6 (Baogong Street), C7 (Wulidun Street), C8 (Wuhu Street), D1 (Mingguang Street), D2 (Shengli Street), D3 (Sanli Street), D4 (Xinglin Street), D5 (Haitang Street), D6 (Heping Street), D7 (Bozhou Street), D8 (Shuanggang Street), as shown in Fig. 5. The results of the population fitting accuracy evaluation are presented in Table 5 and Fig. 6. Among them, 19 streets had a *RE* below 10 %, 15 streets had a *RE* below 20 %, and only two streets, A11 (Jinggang Town) and D2 (Shengli Street), had a *RE* of >30 %, at 31.35 % and 33.93 % respectively. The overall *MRE* was 11.16 %, which indicated good fitting accuracy and effectively reflected the spatial distribution of the downstream population. The number and distribution of the affected populations were extracted based on the simulation results of floods routing and population distribution, as shown in Fig. 7. According to the Hefei Statistical Yearbook for 2020, on average, four people in Hefei own a private car. Assuming that each car seats two people, each residential area was set to half the number of people evacuated by car or walking.

3.2. Screening results of candidate shelters

In this study, sites such as schools, parks, green spaces and squares in four administrative districts, namely Luyang District, Shushan District, Yaohai District and Baohe District, were acquired, from which qualified candidate shelters were obtained according to the screening criteria. Under normal weather conditions, 352 candidate shelters were selected. In extreme rainfall weather, referring to the extremely heavy rainstorm disaster in Hefei in 2020 (Feng et al., 2023; Hefei Emergency Management Bureau, n.d.), roads with an elevation of <13.3 m were set to be impassable with ponding depth of >20 cm. Consequently, 86 inaccessible shelters with zero effective capacity were screened out from 352 candidate shelters, resulting in 266 candidate shelters being ultimately
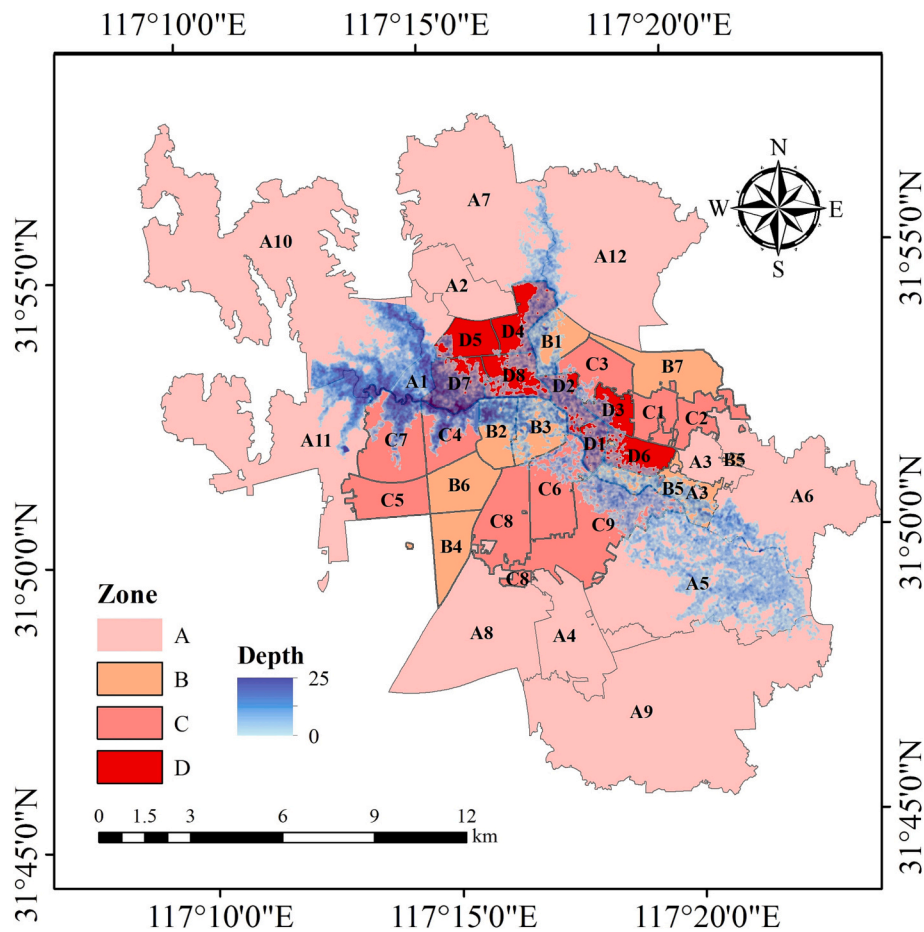
Fig. 5. Simulation results of floods routing and study area zoning.

Table 5
Specific situation of each zone.

Zone	Agglomeration degree	Including the number of streets	Fitting formula	R^2	MRE
I	0.5–2	12	$y = 0.002x_1 + 2707.444x_2 + 6658.254x_3$	0.899	11.09
II	2–2.5	7	$y = 0.004x_1$	0.730	10.49
III	2.5–3	8	$y = 0.005x_1$	0.974	6.98
IV	>3	8	$y = 0.006x_1$	0.750	14.31

Note: x_1 is the DN value (Digital Number) of lights on residential land; x_2 is the area of lights on cultivated land (km^2); x_3 is the area of lights on grassland (km^2).

retained. The screening results for candidate shelters are shown in Fig. 8.

3.3. Results of shelter selection

Prioritizing the use of established and high-level shelters should be considered to reduce construction costs and improve the comfort of the population. Therefore, in Eq. (16), the priority parameters Q_j were set to 1, 1.1, 1.2, and 1.3 for grades I, II, III, and the remaining shelters, respectively (which can be dynamically adjusted according to the needs during application). The 100 groups of shelters selection schemes are initially constructed randomly, and the crossover and variance probabilities in the genetic algorithm were taken as 0.8 and 0.1, respectively (Hu et al., 2022), and the model results tended to stabilize after 5000 iterations after many experimental tests to obtain the pareto solution set. Considering the strong destructive character of the dam failure floods, in the pareto solution set, this study took the solution with the smallest value of objective F_1 (i.e., the highest population transfer efficiency) as the siting solution, and obtained the siting results for different scenarios as shown in Fig. 9 and Table 6.

4. Discussion

According to Table 6, when the population distribution and the effects of extreme rainfall weather were not considered (Scenario 1), 127 locations were selected for population sheltering. Out of these, 63 shelters were designated for people evacuating on foot, 53 for those evacuating by car, and 11 for those evacuating using both methods. After considering only the impact of extreme rainfall (Scenario 2), the number of shelters increased to 183 because of the failure of outdoor capacity or inaccessibility in some shelters. In particular, Linghu Park, Wanghu Park, Lei Street Basketball Park, Hupotan Park and Hefei No. 38 Middle School (Yaohaiwan Campus), which previously accommodated >10,000 people (13,300, 14,900, 12,000, 16,500 and 15,400, respectively) were not selected under this scenario (the locations are shown in A, B, C, D, and E in Fig. 10). This change necessitated a greater number of shelters to accommodate the population that they used to serve. As shown in Table 6, the number of shelters that only accommodated pedestrians increased the most, as slower evacuations of pedestrians were prioritized to shelters closer to them. Among the newly added shelters with a capacity of over 5000, only 5 were arranged to accommodate
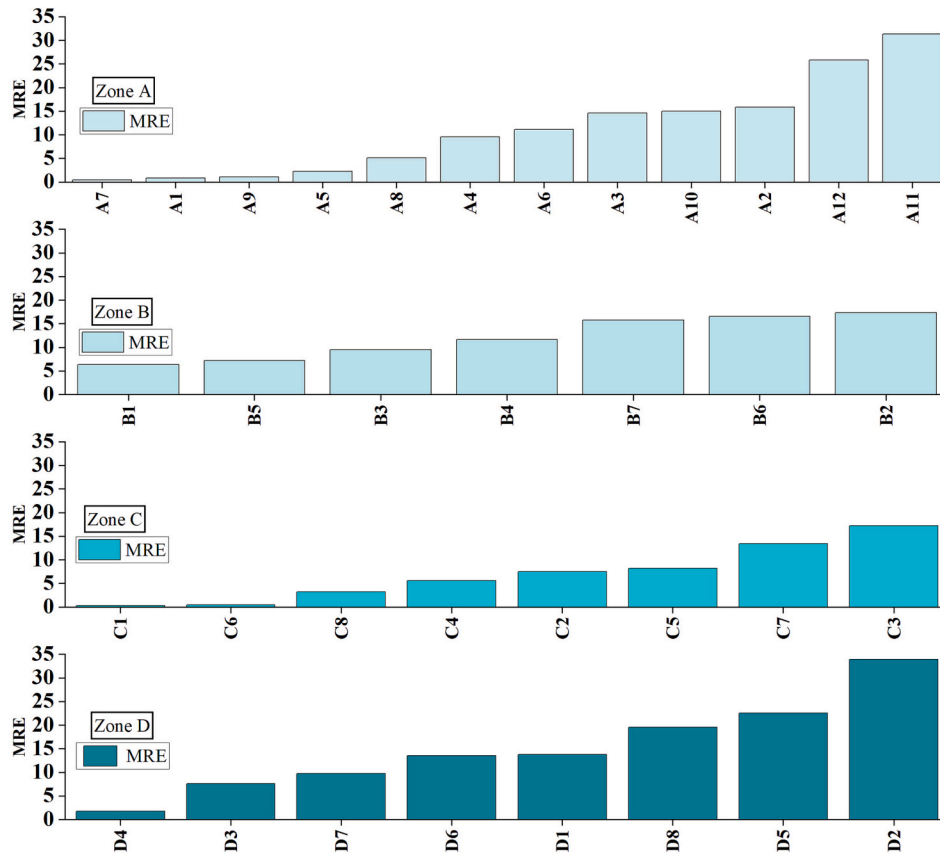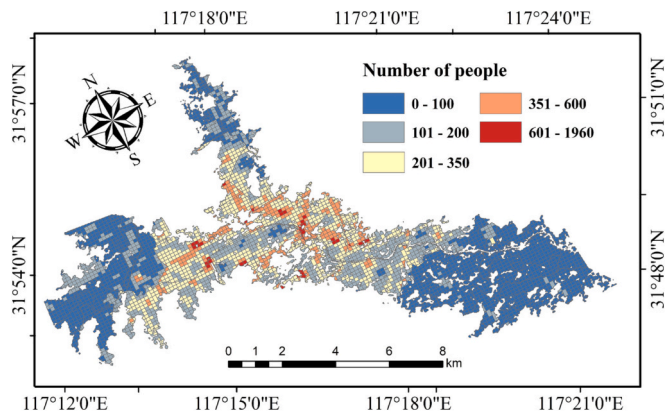
Fig. 6. Relative errors of each street.

Fig. 7. Number and distribution of affected population downstream of reservoirs.

pedestrians because their proximity, whereas 21 were arranged to accommodate drivers because of their distance.

After only population distribution was considered (Scenario 3), the estimated number of affected people increased from 656,000 to 847,000. This increase was due to the inundation areas in potential dam-failure floods being located in densely populated areas. Most shelters that had not reached their maximum capacity showed exhibited an increase in capacity after considering the population distribution. However, five shelters exhibited a decrease in capacity. The capacity of the Botanical Garden decreased from 8700 to 6100. The number of people in the four shelters in Hefei 61st Middle School, Hefei 28th Middle School, South Campus of Hefei 61st Middle School and Angao Square decreased from 2700, 5600, 1600 and 3500 to 0, respectively (F, G, H, I, and J in

Fig. 10). The Botanical Gardens were selected because of their larger capacity (100,000), although they farther away. Several smaller capacity but closer shelters were added after considering the population distribution, such as the 9600-capacity Jinhu Middle School in Hefei (K in Fig. 10) and the 4900-capacity Xincheng Elementary School (L in Fig. 10), to which a portion of the Botanical Garden's population was assigned. Population sharing by smaller capacity but closer shelters was also one of the reasons why the other four shelters were not selected. Another reason was that the populations they accommodated were shared by distant but larger-capacity shelters, such as the University of Science and Technology of China Affiliated High School South Campus (L in Fig. 10).

After considering the population distribution and effects of extreme rainfall (Scenario 4), the number of selected shelters increased to 203. Among these, 131 shelters accommodated populations evacuated on foot, 69 shelters catered to populations evacuated by car, and three shelters accommodated populations evacuated by both methods. The inclusion of these two factors resulted in significant changes in the number of selected shelters, the effective capacity of the shelters, the actual number of people accommodated, the source of the population, and the evacuation methods used. These two factors play crucial roles in determining the shelter selection outcomes. The shelters mentioned above, which varied significantly in the different scenarios, are shown in Fig. 10.

In actual disasters, ensuring safety often requires the evacuation of entire streets or areas. However, this does not mean that considering the population distribution is ineffective. In this study, to reduce computational complexity, we did not use the population of each grid as an evacuation request point. The population distribution simulation was performed only to determine the total number of people affected by the disaster on each street, and the entire street was still used as one evacuation request point. However, in practical applications, each grid can
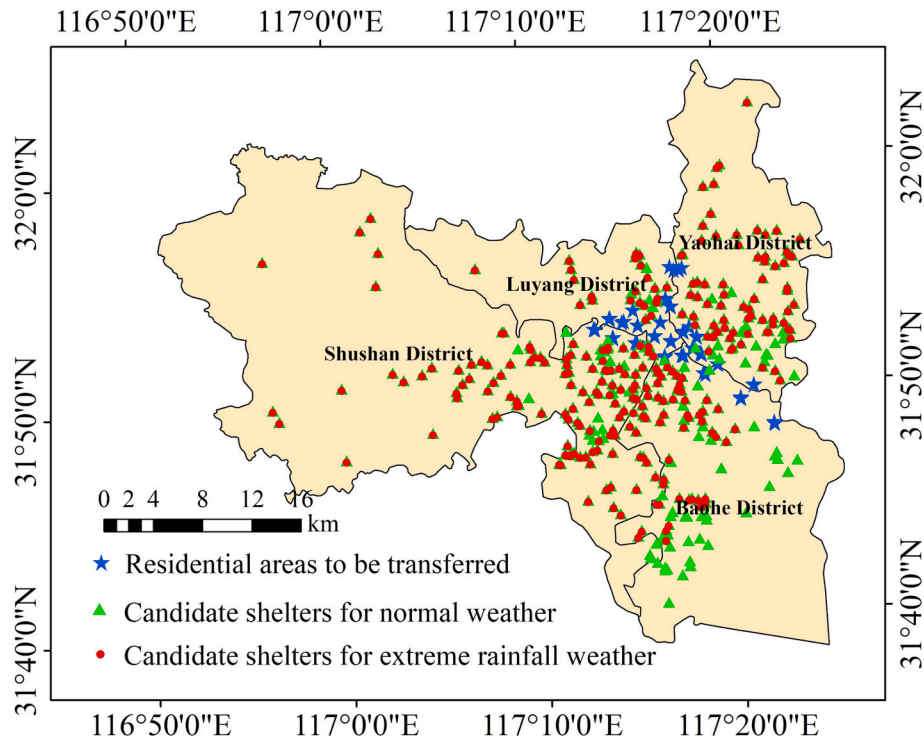
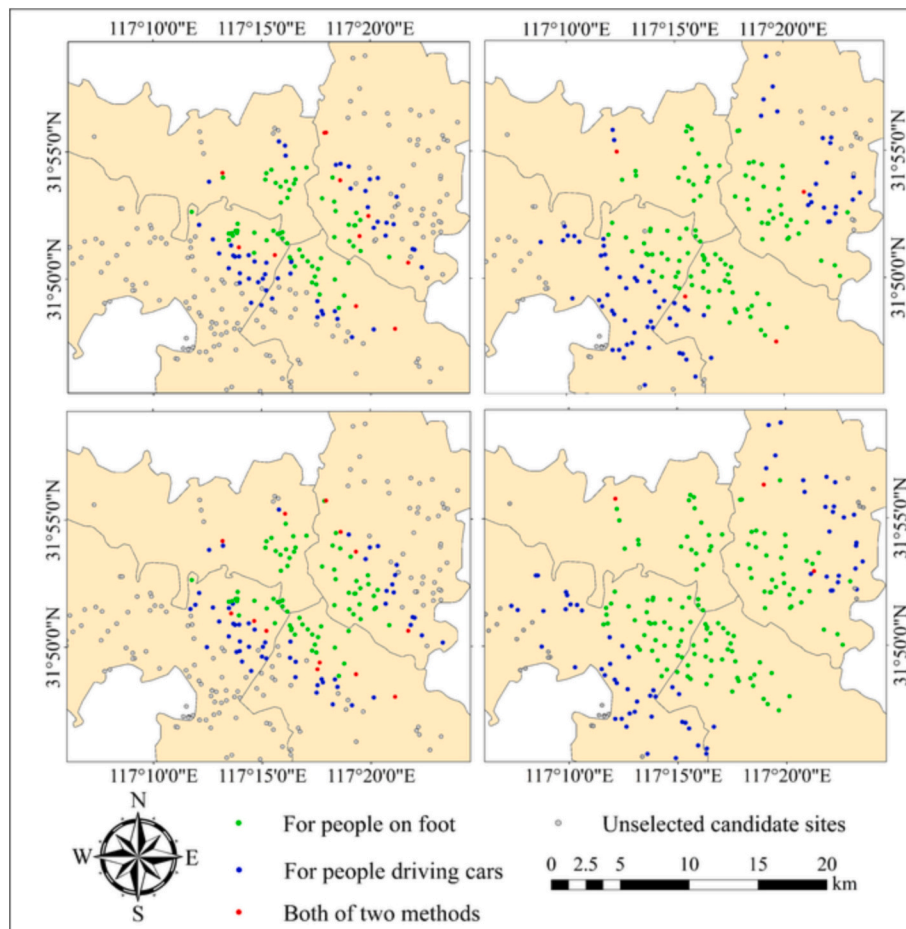**Fig. 8.** Screening results of candidate shelters.

Fig. 9. Results of shelters selection.

Table 6
Comparison of shelters selection results in Different Scenarios.

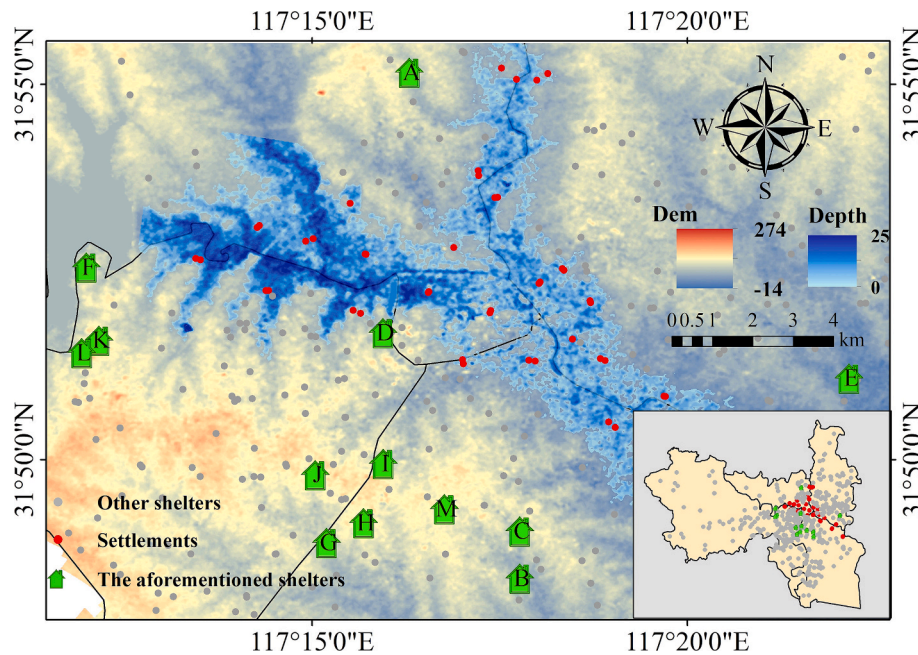| Scenarios	Considering population distribution	Considering extreme rainfall	Number of shelters			
			Selected shelters	Only for people on foot	Only for people driving cars	Both of two methods
1	×	×	127	63	53	11
2	×	√	182	106	72	4
3	√	×	141	73	55	13
4	√	√	203	131	69	3

Fig. 10. Shelters that undergo significant changes in different scenarios.

serve as an evacuation request point by leveraging better hardware configurations and advanced algorithms to enhance the computational efficiency. This enables a more careful reflection of the effects of differences in population distribution on shelter selection, such that the shelters are set up closer to the grid with more people to improve the efficiency of population transfer. In addition, the fitting method based on nighttime lighting and land type data achieved satisfactory results in our research case. However, for some lower middle income countries (LMIC) or regions with low lighting brightness, more factors (such as altitude and terrain) may be added to improve the fitting accuracy.

Predicting the pattern and consequences of dam-failure floods is challenging because of their uncertainty and complexity. Therefore, this study only simulates the dam-failure floods under specific working conditions to highlight the significance of considering population distribution and weather factors when selecting shelters. However, for practical applications, a more detailed analysis of dam-failure floods is necessary.

Reasonable planning and layout optimization of shelters are vital to reducing disaster losses and promoting sustainable urban development. The establishment of a multi-objective mathematical model ensures the scientific natural of the shelter selection scheme, which not only improves the efficiency of emergency transfer and resettlement but also avoids shortages or over-planning of shelters. In addition, government decides shelter planning, and different national conditions lead to different directions for decision-makers. Therefore, follow-up research should consider siting from the perspective of political strategy, which is the key to transforming theoretical achievements into practical applications.

5. Conclusion

Setting up emergency shelters is crucial to effectively reducing the loss of life in the event of dam failure. In this study, the population distribution downstream of a dam was modeled using land type and nighttime lighting data, and combined with the results of HEC-RAS simulations of dam failure flooding to determine the population number and distribution. Qualified candidate shelters were screened based on the screening criteria and their effective capacity and accessibility under in different weather conditions were analyzed and quantified. A shelter selection model was established considering factors such as population transfer efficiency, construction cost, shelter capacity, population distribution differences, and weather conditions. By inputting population and candidate shelter information into the model and using NSGA-II, we obtained shelter selection results for various scenarios. The results indicate the following: (1) The overall MRE of the population distribution simulation results was 11.16 %, which was a good fitting accuracy and can reflect the distribution of most of the population. (2) Normal weather screening yielded 352 qualified candidate shelters, and after considering extreme rainfall weather, 86 sites with zero effective capacity and inaccessible sites were excluded, resulting in 266 sites. (3) In the study area, 141 shelters should be set up under normal weather, whereas 203 shelters should be set up in extreme rainfall weather. (4) The selection of shelters and allocation of population to them undergo significant changes when accounting for population distribution and weather effects. Therefore, the impact of these two factors on dam-failure floods disasters should be considered.

CRediT authorship contribution statement

Yutie Jiao: Conceptualization, Formal analysis, Writing – original draft. **Zongkun Li:** Conceptualization, Funding acquisition, Investigation. **Wei Ge:** Conceptualization, Formal analysis, Funding acquisition, Investigation, Writing – review & editing. **Laihong Jing:** Formal analysis, Methodology. **Meimei Wu:** Methodology, Validation, Writing – original draft. **Te Wang:** Methodology, Writing – review & editing. **Heqiang Sun:** Supervision, Validation. **Jianyou Wang:** Supervision, Validation. **Xiangyang Zhang:** Writing – original draft. **Pieter van Gelder:** Supervision.

Declaration of competing interest

The authors declare that they have no known competing financial interests or personal relationships that could have appeared to influence the work reported in this paper.

Data availability

No data was used for the research described in the article.

Acknowledgements

References

Alessia, F., Renato, V., Paolo, M., 2023. High-resolution 2D shallow water modelling of dam failure floods for emergency action plans[J]. J. Hydrol. 618, 129192 https://doi.org/10.1016/j.jhydrol.2023.129192.

Allahham, L., Mouselli, S., Jakovljevic, M., 2022. The quality of Syrian healthcare services during COVID-19: a HEALTHQUAL approach[J]. Front. Public Health 10, 970922. https://doi.org/10.3389/fpubh.2022.970922.

Amini, H., Asadzadeh, T., Mirhakimi, S., 2022. A new index-based model for site selection of emergency shelters after an earthquake for Iran[J]. Int. J. Disast. Risk Reduct. 77, 103110 https://doi.org/10.1016/J.IJDRR.2022.103110.

Ashlea, B., Lauren, C., Charleen, C., 2023. An exploration of the nearest-shelter assumption in shelter location models[J]. Int. J. Disast. Risk Reduct. 93, 103749 https://doi.org/10.1016/j.ijdrr.2023.103749.

Bahareh, K., Naonori, U., Mohammed, O., et al., 2020. Forest fire susceptibility prediction based on machine learning models with resampling algorithms on remote sensing data[J]. Remote Sens. 12 (22), 3682. https://doi.org/10.3390/rs12223682.

Baharmand, H., Comes, T., Lauras, M., 2019. Bi-objective multi-layer location–allocation model for the immediate aftermath of sudden-onset disasters[J]. Transp. Res. E 127, 86–110. https://doi.org/10.1016/j.tre.2019.05.002.

Baharmand, H., Comes, T., Lauras, M., 2020. Supporting group decision makers to locate temporary relief distribution centres after sudden-onset disasters: a case study of the 2015 Nepal earthquake[J]. Int. J. Disast. Risk Reduct. 45, 101455 https://doi.org/10.1016/j.ijdrr.2019.101455.

Bao, W., Gong, A., Zhang, T., et al., 2023. Mapping population distribution with high spatiotemporal resolution in Beijing using baidu heat map data[J]. Remote Sens. 15 (2), 458. https://doi.org/10.3390/RS15020458.

Chen, T., Pandey, B., Seto, K., 2023. Detecting subpixel human settlements in mountains using deep learning: a case of the Hindu Kush Himalaya 1990–2020[J]. Remote Sens. Environ. 294, 113625 https://doi.org/10.1016/J.RSE.2023.113625.

Church, R., Revelle, C., 1974. The maximal covering location problem[J]. Pap. Reg. Sci. 32 (1), 101–118.

Esmaelian, M., Tavana, M., Arteaga, S., et al., 2015. A multicriteria spatial decision support system for solving emergency service station location problems[J]. Int. J. Geogr. Inf. Sci. 29 (7), 1187–1213. https://doi.org/10.1080/13658816.2015.1025790.

Fang, G., Gao, Z., Tian, L., et al., 2022. What drives urban carbon emission efficiency? – spatial analysis based on nighttime light data[J]. Appl. Energy 312, 118712. https://doi.org/10.1016/J.APENERGY.2022.118772.

Felice, C., Di, C., Lamarucciola, N., et al., 2021. Experimental estimation of energy dissipated by multistorey post-tensioned timber framed buildings with anti-seismic dissipative devices[J]. Sustain. Struct. 1 (2), 000007 https://doi.org/10.54113/j.sust.2021.000007.

Feng, J., Duan, T., Zhou, Y., et al., 2023. An improved nonnegative matrix factorization with the imputation method model for pollution source apportionment during rainstorm events[J]. J. Environ. Manag. 328, 116888 https://doi.org/10.1016/j.jenvman.2022.116888.

Ge, W., Li, Z., Liang, R., et al., 2017. Methodology for establishing risk criteria for dams in developing countries, case study of China[J]. Water Resour. Manag. 31 (13), 4063–4074. https://doi.org/10.1007/s11269-017-1728-0.

Ge, W., Qin, Y., Li, Z., et al., 2020a. An innovative methodology for establishing societal life risk criteria for dams: a case study to reservoir dam failure events in China[J]. Int. J. Disast. Risk Reduct. 49, 101663 https://doi.org/10.1016/j.ijdrr.2020.101663.

Ge, W., Sun, H., Zhang, H., et al., 2020b. Economic risk criteria for dams considering the relative level of economy and industrial economic contribution. Sci. Total Environ. 725, 138–139. https://doi.org/10.1016/j.scitotenv.2020.138139.

Ge, W., Wang, X., Li, Z., et al., 2021. Interval analysis of loss of life caused by dam failure [J]. J. Water Resour. Plan. Manag. 147 (1), 04020098. https://doi.org/10.1061/(ASCE)WR.1943-5452.0001311.

Ge, W., Jiao, Y., Wu, M., et al., 2022. Estimating loss of life caused by dam breaches based on the simulation of floods routing and evacuation potential of population at risk[J]. J. Hydrol. 612, 128059 https://doi.org/10.1016/J.JHYDROL.2022.128059.

Geng, S., Hou, H., Zhou, Z., 2021. A hybrid approach of VIKOR and bi-objective decision model for emergency shelter location–allocation to respond to earthquakes[J]. Mathematics 9, 1897. https://doi.org/10.3390/math9161897.

Hakimi, S., 1964. Optimum locations of switching centers and the absolute centers and medians of a graph[J]. Oper. Res. 12 (3), 450–459. https://doi.org/10.1287/opre.12.3.450.

Hakimi, S., 1965. Optimum distribution of switching centers in a communication network and some related graph theoretic problems[J]. Oper. Res. 13 (3), 462–475. https://doi.org/10.1287/opre.13.3.462.

Hefei Emergency Management Bureau. Notice on announcing the relevant information of emergency refuge places in the City. https://yjj.hefei.gov.cn/public/14391/105414709.html.

Hu, W., Yang, Q., Chen, H., et al., 2022. A novel approach for wind farm micro-siting in complex terrain based on an improved genetic algorithm[J]. Energy 251, 123970. https://doi.org/10.1016/J.ENERGY.2022.123970.

Jakovljevic, M., Sugahara, T., Timofeyev, Y., et al., 2020. Predictors of (in) efficiencies of healthcare expenditure among the leading Asian economies comparison of OECD and non-OECD nations[J]. Risk Manag. Healthcare Policy 13, 2261–2280. https://doi.org/10.2147/RMHP.S266386.

Jakovljevic, M., Lamnisos, D., Westerman, R., et al., 2022. Future health spending forecast in leading emerging BRICS markets in 2030: health policy implications[J]. Health Res. Policy Syst. 20, 23. https://doi.org/10.1186/s12961-022-00822-5.

Jakovljevic, M., Chang, H., Pan, J., et al., 2023. Successes and challenges of China's health care reform: a four-decade perspective spanning 1985—2023[J]. Cost Eff. Resource Alloc. 21, 59. https://doi.org/10.1186/s12962-023-00461-9.

Jeong, D., Kim, M., Song, K., et al., 2021. Planning a green infrastructure network to integrate potential evacuation routes and the urban green space in a coastal city: the case study of Haeundae District, Busan, South Korea[J]. Sci. Total Environ. 76, 143179 https://doi.org/10.1016/j.scitotenv.2020.143179.

Jin, J., Shen, Y., Hu, H., et al., 2021. Optimizing underground shelter location and mass pedestrian evacuation in urban community areas: a case study of Shanghai[J]. Transp. Res. A 149, 124–138. https://doi.org/10.1016/j.tra.2021.04.009.

Kaseb, Z., Rahbar, M., 2022. Towards CFD-based optimization of urban wind conditions: comparison of genetic algorithm, particle swarm optimization, and a hybrid algorithm[J]. Sustain. Cities Soc. 77, 103565 https://doi.org/10.1016/j.scs.2021.103565.

Kilci, F., Kara, B., Bozkaya, B., 2015. Locating temporary shelter areas after an earthquake: a case for Turkey[J]. Eur. J. Oper. Res. 243 (1), 323–332. https://doi.org/10.1016/j.ejor.2014.11.035.

Kotz, M., Levermann, A., Wenz, L., 2022. The effect of rainfall changes on economic production[J]. Nature 601, 223–227. https://doi.org/10.1038/s41586-021-04283-8.

Kreibich, H., Van Loon, A., Schröter, K., et al., 2022. The challenge of unprecedented floods and droughts in risk management[J]. Nature 608, 80–86. https://doi.org/10.1038/s41586-022-04917-5.

Li, B., Xu, Z., Zhang, Y., et al., 2021a. Two-stage multi-sided matching dispatching models based on improved BPR function with probabilistic linguistic term sets[J]. Int. J. Mach. Learn. Cybern. 12, 151–169. https://doi.org/10.1007/s13042-020-01162-y.

Li, Z., Li, W., Ge, W., 2018. Weight analysis of influencing factors of dam break risk consequences[J]. Nat. Hazards Earth Syst. Sci. 18 (12), 3355–3362. https://doi.org/10.5194/nhess-18-3355-2018.

Li, Z., Zhang, Y., Wang, J., et al., 2021b. Impact evaluation of geomorphic changes caused by extreme floods on inundation area considering geomorphic variations and land use types[J]. Sci. Total Environ. 754, 142424 https://doi.org/10.1016/j.scitotenv.2020.142424.

Lv, H., Wu, Z., Guan, X., et al., 2021. The construction of flood loss ratio function in cities lacking loss data based on dynamic proportional substitution and hierarchical Bayesian model[J]. J. Hydrol. 592, 125797 https://doi.org/10.1016/j.jhydrol.2020.125797.

Lv, H., Wu, Z., Meng, Y., et al., 2022. Optimal domain scale for stochastic urban flood damage assessment considering triple spatial uncertainties[J]. Water Resour. Res. 58 (7), 1–20. https://doi.org/10.1029/2021WR031552.

Maryam, G., Hossein, S., Abodosalam, G., et al., 2023. Location-pricing decisions with carbon emission considerations: a behavioral game-theoretic approach[J]. J. Clean. Prod. 422, 138621 https://doi.org/10.1016/j.jclepro.2023.138621.

Ottavia, C., Alessandro, B., Lleana, C., et al., 2021. Design issues for smart seismic isolation of structures: past and recent research[J]. Sustain. Struct. 1 (1), 000001 https://doi.org/10.54113/j.sust.2021.000001.

Ozbay, E., Çavuş, Ö., Kara, Y., 2019. Shelter site location under multi-hazard scenarios [J]. Comput. Oper. Res. 106, 102–118. https://doi.org/10.1016/j.cor.2019.02.008.

Qin, L., Xu, W., Zhao, X., 2020. Typhoon track change–based emergency shelter location–allocation model: a case study of Wenchang in Hainan province, China[J]. Inj. Prev. 26 (3), 196–203. https://doi.org/10.1136/INJURYPREV-2018-043081.

Rahman, M., Chen, N., Islam, M., et al., 2020. Location-allocation modeling for emergency evacuation planning with GIS and remote sensing: a case study of Northeast Bangladesh[J]. Geosci. Front. 12, 101095 https://doi.org/10.1016/j.gsf.2020.09.022.

Ranabhat, C., Jakovljevic, M., Dhimal, M., et al., 2020. Structural factors responsible for universal health coverage in low- and middle-income countries: results from 118 countries[J]. Front. Public Health 7, 414. https://doi.org/10.3389/fpubh.2019.00414.

Resource and Environment Science and Data Center, Institute of Geography Sciences and Natural Resources, 2020. Remote sensing monitoring data of land use in China. http://www.resdc.cn.

Seyed, V., Sadeghi, A., Seo, M., 2023. Application of genetic algorithm in optimization parallel ensemble-based machine learning algorithms to flood susceptibility mapping using radar satellite imagery[J]. Sci. Total Environ. 873, 162285 https://doi.org/10.1016/J.SCITOTENV.2023.162285.

State key Laboratory of information Engineering in Surveying, Mapping and Remotes Sensing. http://59.175.109.173:8888/index.html.

Sun, J., Jin, H., Tsai, F., et al., 2022. A global assessment of sustainable development: integrating socioeconomic, resource and environmental dimensions[J]. Front. Energy Res. 10, 816714 https://doi.org/10.3389/fenrg.2022.81671.

Tan, M., Li, X., Li, S., et al., 2018. Modeling population density based on nighttime light images and land use data in China[J]. Appl. Geogr. 90, 239–247. https://doi.org/10.1016/j.apgeog.2017.12.012.

Toregas, C., Swain, R., ReVelle, C., et al., 1971. The location of emergency service facilities[J]. Oper. Res. 19 (6), 1363–1373. https://doi.org/10.1287/opre.19.6.1363.

Trivedi, A., 2018. A multi-criteria decision approach based on DEMATEL to assess determinants of shelter site selection in disaster response[J]. Int. J. Disast. Risk Reduct. 31, 722–728. https://doi.org/10.1016/j.ijdrr.2018.07.019.

US Army Corps of Engineers, 2016. Hydrologic Engineering Center. HEC-RAS 5.0 2D Modeling User's Manual.

Wang, L., Wang, S., Zhou, Y., et al., 2018. Mapping population density in China between 1990 and 2010 using remote sensing[J]. Remote Sens. Environ. 210, 269–281. https://doi.org/10.1016/j.rse.2018.03.007.

Wang, T., Li, Z., Ge, W., et al., 2022a. Calculation of dam risk probability of cascade reservoirs considering risk transmission and superposition[J]. J. Hydrol. 609, 127768 https://doi.org/10.1016/J.JHYDROL.2022.127768.

Wang, T., Li, Z., Ge, W., et al., 2022b. Risk assessment methods of cascade reservoir dams: a review and reflection[J]. Nat. Hazards 115 (2), 1601–1622. https://doi.org/10.1007/S11069-022-05609-Z.

Wang, T., Li, Z., Ge, W., et al., 2023a. Rank classification method for cascade reservoirs considering scale, benefits, and risk consequences[J]. J. Hydrol. 623, 129856 https://doi.org/10.1016/j.jhydrol.2023.129856.

Wang, T., Li, Z., Ge, W., et al., 2023b. Risk consequence assessment of dam breach in cascade reservoirs considering risk transmission and superposition[J]. Energy 15 (265), 126315. https://doi.org/10.1016/J.ENERGY.2022.126315.

Weber, A., 1929. Theory of the location of industries (trans: Friedrich, C.J. from Weber's 1909 book). Chicago: The University of Chicago Press.

Weber, M., Seaman, Y., Stewart, N., et al., 2018. Census-independent population mapping in northern Nigeria[J]. Remote Sens. Environ. 204, 786–798. https://doi.org/10.1016/j.rse.2017.09.024.

Wood, N., Schmidtlein., 2013. Community variations in population exposure to near-field tsunami hazards as a function of pedestrian travel time to safety. Nat. Hazards 65 (3), 1603–1628. https://doi.org/10.1007/s11069-012-0434-8.

Wu, B., Yang, C., Wu, Q., et al., 2023. A building volume adjusted nighttime light index for characterizing the relationship between urban population and nighttime light intensity[J]. Comput. Environ. Urban. Syst. 99, 101911 https://doi.org/10.1016/J.COMPENVURBSYS.2022.101911.

Wu, M., Wu, Z., Ge, W., et al., 2021. Identification of sensitivity indicators of urban rainstorm flood disasters: a case study in China[J]. J. Hydrol. 599, 126393 https://doi.org/10.1016/j.jhydrol.2021.126393.

Xu, Y., Zhang, L., 2009. Breaching parameters for earth and rockfill dams[J]. J. Geotech. Geoenviron. Eng. 135 (12), 1957–1969. https://doi.org/10.1061/(ASCE)GT.1943-5606.0000162.

Yao, J., Zhang, X., Murray, A., 2017. Location optimization of urban fire stations: access and service coverage[J]. Comput. Environ. Urban. Syst. 73, 184–190. https://doi.org/10.1016/j.compenvurbsys.2018.10.006.

Zhang, H., Ge, W., Zhang, Y., et al., 2023a. Risk management decision of reservoir dams based on the improved life quality index[J]. Water Resour. Manag. 37, 1223–1239. https://doi.org/10.1007/s11269-023-03426-y.

Zhang, J., Song, G., Gong, D., et al., 2017. Analysis of rainfall effects on road travel speed in Beijing, China[J]. IET Intell. Transp. Syst. 12 (2), 93–102. https://doi.org/10.1049/iet-its.2017.0039.

Zhang, X., Qiao, W., Xiao, Y., et al., 2023b. Analysis of regional flooding in the urbanization expansion process based on the SWMM model[J]. Nat. Hazards 117, 1349–1363. https://doi.org/10.1007/S11069-023-05906-1.

Zhao, S., Liu, Y., Zhang, R., et al., 2020. China's population spatialization based on three machine learning models[J]. J. Clean. Prod. 256, 120644 https://doi.org/10.1016/j.jclepro.2020.120644.

Zhao, X., Xu, W., Ma, Y., et al., 2017. Relationships between evacuation population size, earthquake emergency shelter capacity, and evacuation time[J]. Int. J. Disast. Risk Sci. 8, 457–470. https://doi.org/10.1007/s13753-017-0157-2.

Zhong, G., Zhai, G., Chen, W., et al., 2022. Optimization of shelter location based on a combined static/dynamic two-stage optimization methodology: a case study in the central urban area of Xinyi City, China[J]. ISPRS Int. J. Geo Inf. 11, 262. https://doi.org/10.3390/IJGI11040262.

Zhu, Y., Tang, H., 2023. Automatic damage detection and diagnosis for hydraulic structures using drones and artificial intelligence techniques[J]. Remote Sens. 15, 615. https://doi.org/10.3390/RS15030615.